



# Bulletin of the Mineral Research and Exploration

<http://bulletin.mta.gov.tr>



## Modeling of the complex hydrocarbon traps by the shot domain acoustic finite difference method and data-processing

Şerife BOĞAZKESEN<sup>a\*</sup> and Hakan KARSLI<sup>b</sup>

<sup>a</sup>Atatürk University, Faculty of Engineering, Department of Civil Engineering, Erzurum, Türkiye

<sup>b</sup>Karadeniz Technical University, Faculty of Engineering, Department of Geophysics, Trabzon, Türkiye

Research Article

Keywords:

Finite Difference Method, Data Processing, Hydrocarbon Traps, Seismic Modeling, Synthetic Shot.

### ABSTRACT

Numerical modeling studies have a widespread application in exploration seismology in order to understand the seismic reflection responses of hydrocarbon traps formed in relation to tectonic structure, lithological changes and unconformities in complex geological environments and to develop effective data processing strategies. In this study, the seismic modeling of two important hydrocarbon trap models (Granite Wash and Normal Fault Trap) was performed by the Finite Difference Method (FDM), which provides the solution of the acoustic wave equation. Seismic data models were carried out in the pre-stack shot environment, and the obtained shot data were passed through appropriate data-processing stages to obtain stack and migration (zero offset) sections. By converting the obtained migration sections to depth, the spatial location and dimensions of hydrocarbon traps on the section were determined and it has been observed that they are compatible by comparing with the initial geological models. Thus, the seismic responses of hydrocarbon trap structures were learned, the importance of data processing was understood, and zero offset cross-sections were obtained by processing of the generated synthetic shot records. Accordingly, it was observed that it is appropriate to make more and frequent shots in the investigation of granite wash type traps which are thin and short-width, whereas it is useful to make relatively less frequent shots in order to reduce the scattering intensity caused by the discontinuities of the fault type structures. Consequently, it is thought that before the field study for the hydrocarbon exploration, the modeling of the pre-stack shot instead of the post-stack modeling (zero offset) will contribute to the development of the data processing stages and the testing of the seismic section interpretation. In the future, such synthetic models and data processing will be developed for different complex trap structures and real data.

Received Date: 15.03.2021

Accepted Date: 20.08.2021

## 1. Introduction

Hydrocarbon (petroleum, natural gas, and coal) resources account for 86% of the world's energy consumption. In Türkiye, this rate reaches 92% (TPAO, 2022). Therefore, investments and interest in the exploration and discovery of hydrocarbon traps still remain more important. As a result, great deals of

effort are put in towards further developing onshore and offshore activities both in Türkiye and in the globe through the usage of advanced technology and effective methods.

A hydrocarbon trap is defined as a porous and permeable rock with any geometric shape that contains structurally or stratigraphically formed oil and natural

Citation Info: Boğazkesen, Ş., Karslı, H. 2022. Modeling of the complex hydrocarbon traps by the shot domain acoustic finite difference method and data-processing. Bulletin of the Mineral Research and Exploration 168, 93-109. <https://doi.org/10.19111/bulletinofmre.985502>.

\*Corresponding author: Şerife BOĞAZKESEN, [serifebogazkesen@atauni.edu.tr](mailto:serifebogazkesen@atauni.edu.tr)

gas, or both. As is known, the most powerful method for detecting the location of hydrocarbon traps of different scales at different depths of the Earth is the seismic reflection. Studies of hydrocarbon traps by seismic reflection method include data collection from the field with multi-source system, multi-receiver systems, processing and interpretation of collected data with up-to-date software suitable for the purpose. The interpretation allows the determination of structures and hydrocarbon traps by taking into account the structural and stratigraphic principles. At the same time, to know how the seismic responses of structural and stratigraphic hydrocarbon traps will be in general provides important contributions to the interpreter for the interpretation of seismic sections. Also, complexity of the geological structures in which the traps are located and omissions in data processing processes or the deficiencies and errors in the parameter selection will adversely affect the quality of the seismic sections to be interpreted.

Seismic reflection response of hydrocarbon traps is performed by numerical modeling of acoustic or elastic seismic wave propagation within the designated ground model and referred to as seismic modeling. The seismic modeling is commonly used to plan for collecting good quality seismic data (Gjøystdal et al., 2007; Robertson et al., 2015) and to improve seismic data processing workflow on complex geological structures (Aminzadeh et al., 1997; Gjøystdal et al., 2007; Huang et al., 2010; Özbek et al., 2010) and they are also extremely useful for associating an interpreted geological model with real data. An important application on this field is the experimentation of different geological models to study structural and stratigraphic problems encountered during seismic interpretation (Sayers and Chopra, 2009). Under the circumstances, seismic modeling is especially used and especially the use of seismic modeling to check the validity of interpretation in complex geological situations. Thus, seismic modeling is one of the most reliable way to investigate the validity of models representing different types of structural traps and to find the best fit with real seismic data (Lingrey, 1991; Morse et al., 1991; Alaei, 2006; Alaei and Petersen, 2007).

Geological models are constructed from lithological units containing one-dimensional (1D),

two-dimensional (2D), or three-dimensional (3D) P, S-wave velocities and intensities. Geological ground models can include simple structures with horizontal and inclined plane decals, and also complex structures with discontinuities in the lateral and vertical directions. Just the same, hydrocarbon-containing geological structure models usually consist of the complexities of their structural and sedimentary conditions. Geological modeling of wave propagation in such environments and the actual terrain data with different advantages and disadvantages in comparison with ray tracing, discrete wave number, finite differences, finite elements, etc although many methods are employed, such as numerical, Finite Difference Method (FDM) can provide successful results in very complex environments. FDM, the most well-known method that provides a high-precision and complete numerical solution of partial differential equations, is widely used in seismic modeling studies FDM, the most well-known method that provides a high-precision and complete numerical solution of partial differential equations, is widely used in seismic modeling studies (Kelly et al., 1976; Virieux, 1986; Igel et al., 1995; Etgen and O'Brien, 2007; Bansal and Sen, 2008; Liu and Sen, 2009; Robertson et al., 2015; Talukdar and Behera, 2018). The process of wave propagation modeling with FDM started in parallel with the development of computer technologies in the 1960s, and the fact that it began to be used in wave propagation problems attracted a lot of attention (Alterman and Karal, 1968; Boore, 1970; Ottaviani, 1971). These methods provide a full-wave field solution and include all wave fields such as reflection, scattering, repetition and surface wave. So far, this method has solved many problems such as accuracy, stability and high-order operator arrangement for calculating numerical derivatives (Zhang and Zhang, 2007; Liu and Sen, 2009). For this reason, FDM has become the preferred modeling method for highly complex geological models, especially since it provides accurate amplitude information. Geiger and Daley (2003) used Acoustic Finite Difference (AFD) equations to simulate acoustic fields in variable density and velocity environments and numerical solutions of these equations were performed in MatLab (Matrix Laboratory) environment. In the solution, the researchers generated the first Marmousi data set using the 5-point central finite difference

algorithm. However, Nejadi and Hashemi (2012) made zero-expansion seismic modeling of four different geological models with FDM in their study and to test the accuracy of the obtained section, they compared it with the interpreted sections. With this approach Many researchers who study complex geological and bedrock environments have adopted this method (Blake et al., 1999; Bohlen et al., 2003; Jinhua et al., 2009; Ahmadi et al., 2013). After the FDM, the scattering is brought to their real position by applying stack migration, and the real underground image is obtained correctly. Talukdar and Behere (2018) used the FDM to obtain the artificial shooting data of complex geological underground structures under uneven thick basaltic rocks, by applying Kirchhoff pre aggregation time migration and post aggregation depth migration to these model data, they successfully visualized the changes of inclined faults and lithology.

Seismic reflection modeling is usually carried out on the aggregation and / or migration profile (zero expansion profile) obtained after a series of data processing on the field from collected data. The most important reason for this is to save computing time and computer storage capacity, and also avoid intensive data processing to create zero extension segments (stacking and migration segments) starting from shot point data. However, with the developments leading to increasing computer speed, power and enhanced data processing software, and studies on shot point record modeling has been increasing in recent years. Considering that the seismic data are collected from the field with shot point receiver array in a certain order, modeling the shot point records, and then processing the shot point records to obtain stacking and / or migration profiles is a more realistic method of seismic data interpretation.

In this study, it was aimed to model the shot records of geological ground models (granite wash and normal fault trap) that may be complex hydrocarbon traps with FDM and to obtain zero-opening sections with data processing applications. To this end, Matlab based software developed by Youzwishen and Margrave (1999) is used to calculate manual artificial shooting data and arrange it according to the purpose. The calculated shot model data were processed with ProMax software and Kirchhoff time migration cross

sections were obtained after stacking. The indication of hydrocarbon trap was examined on the zero expansion section thus obtained. In addition, the compatibility between reflection levels and geological model was also compared.

## 2. Material and Method

### 2.1. Acoustic Finite Difference Method (AFDM)

FDM is a numerical solution of differential wave equation used to calculate seismic wave propagation in any geological model. When this method is applied to acoustic wave equation, it is called AFDM, and when it is applied to elastic wave equation, it is called Elastic Finite Differences Method (EFDM). In this article, the acoustic equation given in Equation 1 is solved and modeled by FDM. The seismic wave field is calculated at each grid point shown in Figure 1 by providing an approximation with finite difference formulas that are derivatives of the wave equation and solving the resulting difference equation recursively. However, the number of (analytical) solutions of the wave equation is rare, and usually approximate numerical solutions are preferred for wave field modeling. Under this background, FDM has developed into a numerical technique in artificial seismic data calculation and has been widely used (Marfurt, 1984; Krebes and Lee, 1994; Manning and Margrave, 1998; Youzwishen and Margrave, 1999; Carcione et al., 2002; Margrave, 2003; Moczo et al., 2007).

AFDM provides the direct solution of the partial differential acoustic wave equation given by Equation 1 under certain initial and boundary conditions. The method provides for the possibility of obtaining the propagation of acoustic waves in complex geological models from simple to complex. The 2D scalar (numerical) wave equation ( $x, z$ ) of the method can be written in Cartesian (perpendicular) coordinates as follows (Lines et al., 1999).

$$\frac{\partial^2 \phi(x,z,t)}{\partial t^2} = v^2(x,z) \nabla^2 \phi(x,z,t) \quad (1)$$

In Equation 1,  $x$  and  $z$  are the horizontal and vertical distances (meter-m), respectively, on the grid network,  $t$  is two-way travel times (second-s),  $\nabla^2$  is the velocity of the medium in which the wave propagates (meters/second-m/s), Laplace;  $\phi(x, z, t)$  and wave

potential or represents the acoustic wave field. The Laplace processor  $2B \nabla^2$  is given by the Equation 2.

$$\nabla^2 \phi = \frac{\partial^2 \phi}{\partial x^2} + \frac{\partial^2 \phi}{\partial z^2} \quad (2)$$

The Laplace operator can be calculated approximately using second-and fourth-degree derivative approximations with central difference operators. These approaches are using 5 and 9 grid points, respectively. In this study, Equation 3, a 9 grid-point fourth-degree Laplace operator approximation, was used by Youzwishen and Margrave (1999) because it provides accuracy and broadband solution, although it increases the calculation time.

$$\nabla^2 \phi \approx \frac{-\phi(x+2,z) + 16\phi(x+1,z) - 30\phi(x,z) + 16\phi(x-1,z) - \phi(x-2,z)}{12\Delta x^2} + \frac{-\phi(x,z+2) + 16\phi(x,z+1) - 30\phi(x,z) + 16\phi(x,z-1) - \phi(x,z-2)}{12\Delta z^2} \quad (3)$$

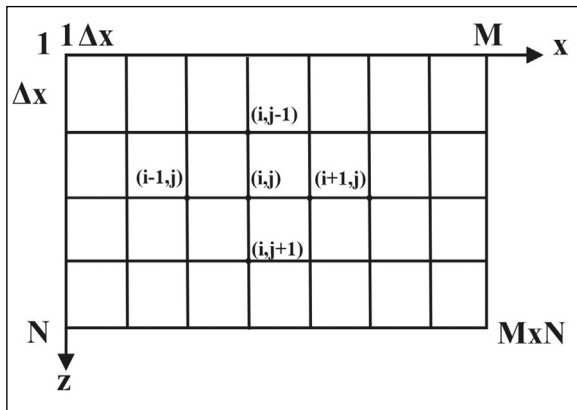


Figure 1- Grid mesh suitable for central finite difference derivative approach. Here,  $\Delta x$ : the grid spacing in the x direction,  $M$ : the number of grids in the x direction,  $\Delta z$ : grid spacing in the z direction,  $N$ : number of grids in the z direction,  $i$ : coordinate x and  $j$ : it represents the z coordinate.

As shown in Figure 1, any point  $(i, j)$  on the grid network is called a network point. According to this point, the points  $(i + 1, j)$  and  $(i-1, j)$  are located to the right and left, while the points  $(i, j + 1)$  and  $(i, j-1)$  represent the points located above and below. If the network used is a regular network, network points can be easily expressed. For example, for a network such as in Figure 1, the network points are as follows

$$x_i = i.\Delta x_i \quad i = 0,1,2,\dots, M$$

$$z_j = j.\Delta z_j \quad j = 0,1,2,\dots, N$$

In such solutions, if an insufficient number of grid points per wavelength is used, an artificial grid

dispersion (scattering) is formed (Holberg, 1987), and this is an important numerical problem. The practical solution to overcome this problem is to choose the grid spacing as small as possible. However, this may increase the calculation time (Youzwishen and Margrave, 1999). In practice, the grid ranges can be different, as they will be taken equal horizontally and vertically ( $\Delta x = \Delta z$ ). However, the stability condition for the fourth-degree approximation, which includes the ambient speed, sampling time, and grid spacing, is as shown in Equation 4.

$$\frac{v_{max}\Delta t}{\Delta x} \leq \sqrt{\frac{3}{8}} \quad (4)$$

Here;  $V_{max}$  is the maximum velocity (meters/second-m/s),  $\Delta t$  is the temporal sampling interval (sec-s), and  $\Delta x$  is the spatial sampling interval (meter-m) ( $\Delta x = \Delta z$ ). Calculation of the time derivative on the left side of Equation 1 using the quadratic central differences approach is given in Equation 5.

$$\frac{\partial^2 \phi}{\partial t^2} = \frac{\phi(t+\Delta t) - 2\phi(t) + \phi(t-\Delta t)}{\Delta t^2} \quad (5)$$

If Equations 3 and 5 are substituted into the numerical wave equation in Equation 1, the wave field at time  $t+\Delta t$  can be solved iteratively in Equation 6 given below.

$$\phi(x, z, t + \Delta t) \approx (2 + \Delta t^2 V(x, z)^2 \nabla^2) \phi(x, z, t) - \phi(x, z, t - \Delta t) \quad (6)$$

In Equation 6,  $\phi$  is the P-wave potential. Equation 6 shows that if the wave field is known at time  $t$  and  $t-\Delta t$ , the wave field at time  $t+\Delta t$  can be calculated. This process is called time stepping and snapshot of the wave propagation at each time. Paying close attention, the wave field is simply removed at time  $t-\Delta t$ , while the Laplace processor is applied to the wave field at time  $T$ . In order for Equation 6 to be used in each time step, it must be defined in advance at times  $t=0$  and  $t=\Delta t$ . This usually requires simply defining a source function or wavelet. In this study, a zero-phase Ricker waveguide was used as the source.

### 3. Geological Models Used

In the conducted researches, many types of traps have been found, which are formed in the form of structural, stratigraphic and their composition. A classification of all three types of traps was made by Hyne (1984). Of these, a stratigraphic (granite

wash) and a structural (normal fault) trap sample were selected, and modeling of shot records and data processing were performed using by FDM. The ground models of the selected trap types are multilayer structures and contain multiple topographic interfaces.

The information about the source function, spatial and temporal calculation parameters used in granite wash and normal fault trap modeling is given in Table 1 below. Reflective decals for modeling were digitized and depth, distance and velocity information were introduced into the modeling software. Attention has been paid to the fact that ground models represent real complex environments. The change in the density values of the layers was taken as constant ( $\rho=2.0 \text{ g/cm}^3$ ), since it was very small compared to the seismic wave velocity.

Table 1- Parameters used for modelling.

Granite Wash/Normal Fault Trap Model	
Profile length (m)	2000
Maximum depth (m)	1000
Receiver interval (m)	10
Shot interval (m)	40
Number of shots	46/25
Number of receivers	201
Max. velocity (m/s)	4000
Min. velocity (m/s)	2000
Max. offset (m)	2000
Min. offset (m)	100
Calculation time step (ms)	0.02
Sampling time (ms)	4
Record length (ms)	1000
Minimum Phase Ricker Source Wavelet (Hz)	30

### 3.1. Granit Wash Trap Model

The Granite Wash trap model, which is a type of stratigraphic trap, has been the target of petroleum research and development studies along with the discovery of oil (Sproule, 1956). A significant amount of hydrocarbons in Granite Wash traps accumulates in low-permeable traps, unlike conventional medium-high-permeable oil traps. These hydrocarbon sources are called unconventional sources and according to the classification of Hyne (1984), they are known as non-traditional stratigraphic tight gas-sand traps. The traps of this type shown in Figure 2 are sandstones

associated with decomposed granite rock and are deep structures (Dec et al., 1996). Underground geological structures containing such hydrocarbon traps are quite complex and do not have similar characteristics to, so it can be quite difficult to identify and define them by seismic surveys.

Figure 2 shows a model of a granite wash trap in a multilayer medium. The model underlying the granite rocks cover to 2700 m/s velocity unit (porous and permeable sandstone, limestone, dolomite, or fractured rock may be) for the peak point on each side from the velocity of 1200 m/s on both sides from the apex is designed to contain (turquoise blue color). However, these trap velocities 2650 m/s (between brown 70-850 m units), 2500 m/s (light color open between 500-600 m units) and 2580 m/s (600-750 m and yellow colored between 400-500 units; non-permeable marl, shale, salt, or mikritik limestone) rocks that covered and locked away. Other units reached the surface by deposited conformably in accordance with the overburden rock (the yellow-colored unit between 400-500 m) with an anticline structure towards the surface. The velocity of the surface layer is 1000 m/s, thickness is 150 m on the left side, 50 m in the middle and 125 m on the right side. In addition, source receiver intervals are shown on veolocity-depth models.

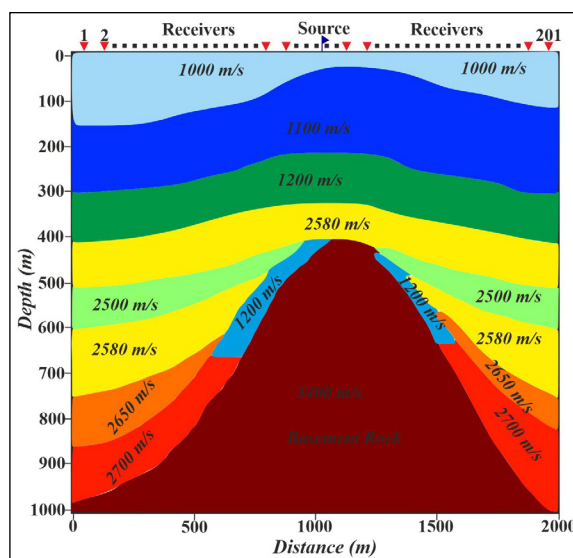


Figure 2- Granite wash trap model. 201 receivers were used. The source receiver (red triangles) layout is shown, with the shot position (dark blue flag) right in the middle of the line.

Examples of 46 shot records calculated according to the parameters in Table 1 for the geological model in Figure 2 are (1., 10., 19., 28., 37., and 46th.). Automatic Gain Control (OGC) is applied and shown in Figure 3. The main reflections can be identified on the shot records, but the reflections from under and above the trap are quite difficult to recognize due to interference. This can be attributed to reasons such as the trap structure is not thick enough, the wavelet used is low frequency, and the grid spacing of the finite difference scheme is wide. Since the main goal of this study is to determine the trap structure by processing data of this complexity, no further improvement has been made in modeling.

### 3.2. Normal Fault Trap Model

Normal fault type traps are structural traps that are curved, formed as a result of the intersection of two faults or the intersection of many faults. Normal fault trap formations occur when the blocks of the fault move in such a way as to prevent the migration of oil. For example, an impermeable and sealed formation on one side of the fault may move in the opposite direction to the oil-field formation on the other side; In this case, the impermeable layer blocks the flow of oil and an oil pool forms against the fault (Biddle and Wielchowsky, 1994). An exemplary normal fault trap

is shown in Figure 4. In this model, oil is placed inside the trap structures (1500 m/sec - turquoise blue color) and covered with overburden rock (2580 m/sec - light green color). However, source receiver intervals are shown on velocity-depth models. In general, although frequent shots provide more common midpoint reflection (folding), it has been observed that frequent interval shots in areas close to discontinuity zones also increase the scattering intensity and deteriorate

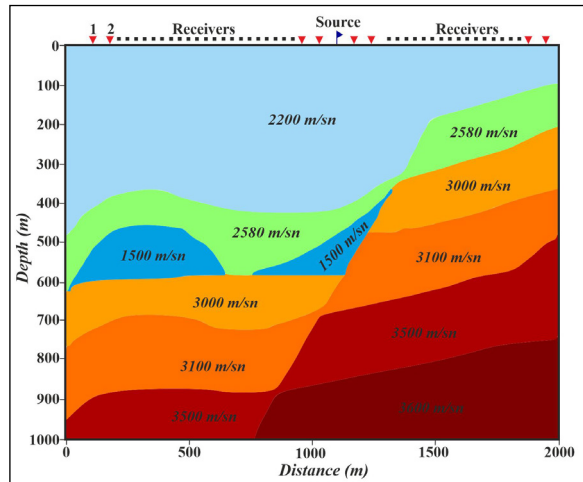


Figure 4- Normal fault trap model 201 receivers were used. The source receiver (red triangles) layout is shown, with the shot position (dark blue flag) right in the middle of the line.

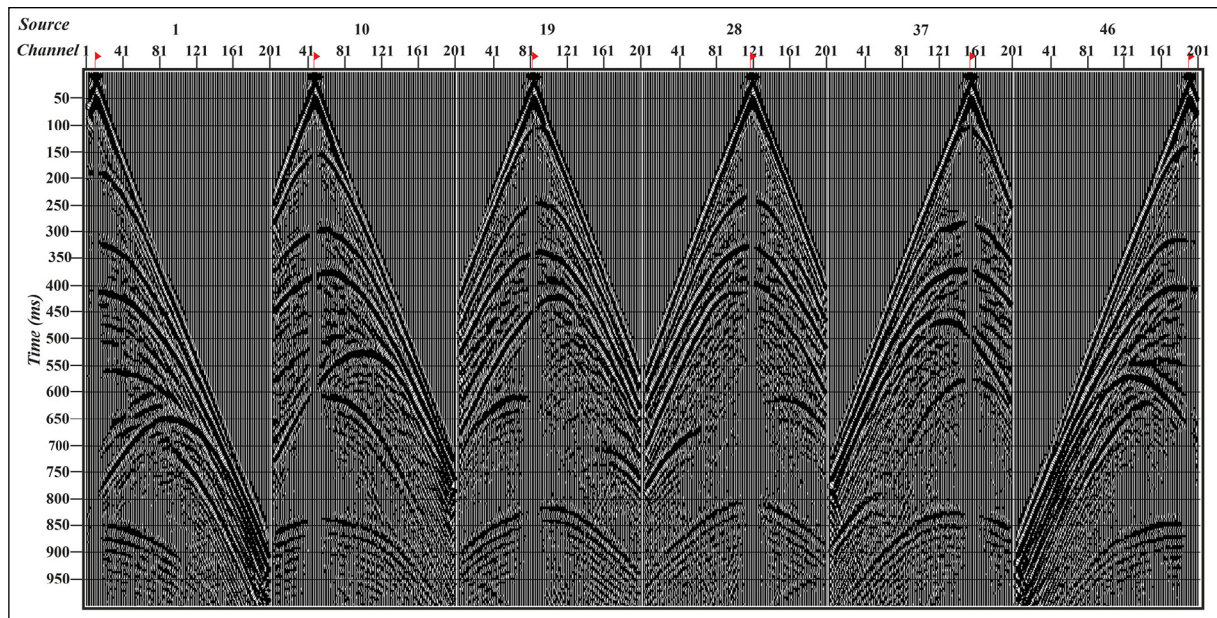


Figure 3- Raw shot groups loaded with 1st, 10th, 19th, 28th, 37th and 46th geometry calculated for the granite wash model. The red flag indicates the seismic source (shot point).

the data quality. For this reason, the number of throws has been reduced to 25, unlike granite wash modeling in the modeling of seismic throw records of a normal fault. Therefore, the number of throws has been reduced to 25, unlike granite wash modeling in the modeling of seismic throw records of a normal fault. Examples of 25 shot records calculated for the normal fault trap model in Figure 4 are presented in Figure 5.

#### 4. Data Processing

The processing of the calculated shot records was carried out using ProMax software.

In this context, the data-processing workflow aimed at obtaining a zero-offset seismic cross-section by suppressing the noise contained in the shot recordings and regulating the reflections, as well as strengthening

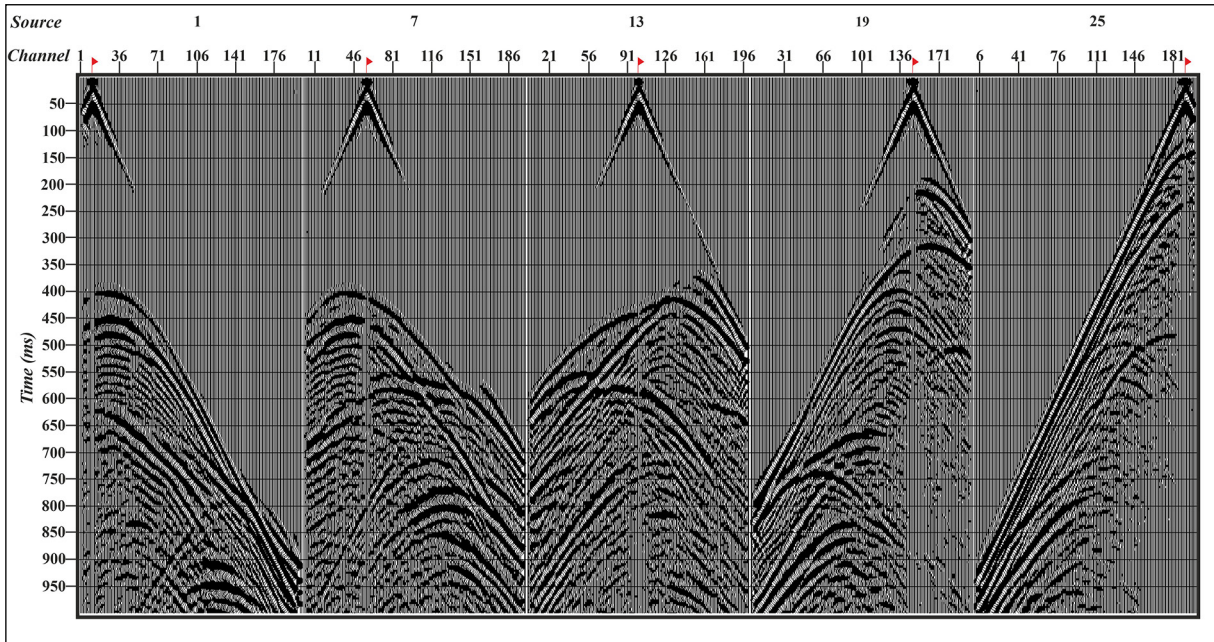


Figure 5- Raw shot groups loaded with 1st, 7th, 13th, 19th and 25th geometry for the normal fault trap model. The red flag indicates the seismic source (shot point).

Table 2- Processes that can be implemented in the data-processing workflow and the reasons for their implementation.

Applied Process	Reasons for Application
Data Loading	Data Reading
Geometry Set Up	Introducing Source and Receiver Positions to the Program
Top Mute	Muting Arrival of Direct Waves
Bandpass Filter (Ormsby Filter)	Filtering Low and High Frequency Noises
Predictive Deconvolution	Suppressing Multiple Reflections/Increasing Temporal Resolution
Bandpass Filter (Ormsby Filter)	Attenuation of High Frequency Noises Strengthened After Deconvolution
Common Midpoint (CMP) Sorting	Creating Common Midpoint Trace Gather
Velocity Analysis	Obtaining RMS (Root Mean Square) Velocity Functions at Each CMP Point for The Best Quality Stacking.
Normal Moveout (NMO) Correction	Moving Pre-Stacking Reflections to Zero Offset Time
Stacking	Overlap of NMO Applied CMP Data
Kirchhoff Time Migration	Elimination of Scattering, Moving Reflections from Curved Interfaces to their Correct Geometric Location
Depth Conversion	Converting Time Axis to Depth
Imaging - Automatic Gain Control (AGC) has been implemented.	Equivalent Amplitudes for Display Purposes

the primary reflections from the reflective surfaces, is given in Table 2. Primary reflections are extremely affected both by scattering and by interference from leaking edge reflections despite the absorbing condition. Therefore, the data-processing stages were applied by selecting the most appropriate parameters.

#### 4.1. Processing Granite Wash Artificial Data

The 46 synthetic data obtained in the granite wash modeling were processed according to the workflow specified in Table 2. After reading the data and the geometric information was defined, the first arrival wave fields (direct ingoing waves and refraction waves) were tried to be cleaned by cutting from the top. However, as can be seen from the shot records in Figure 3, these initial arrivals are quite intertwined with shallow reflections. Therefore, deleting the first destinations from such data requires a lot of attention, otherwise shallow reflections can be damaged. If these initial arrivals are not sufficiently removed, they prevent the focus of speed contours at shallow levels, especially in speed analysis, and can create quite a problem.

However, although the model shot data does not contain low-frequency surface waves and high-frequency noise, processing noise (artifact) may

occur due to data modeling. A band-pass filter with cut-off frequencies of [10 16 60 80] Hz was applied to filter these noises and preserve the useful spectral band of the data (Figure 6). The cut-off frequencies were determined by examining the spectral content of the data and determining which frequency range the useful spectral information was. For this purpose, the pre-band pass filter (Figures 7a and 7b) and post-filter (Figures 7c and 7d) of shot recording No. 1 were compared. The determined filter cut-off frequencies are shown on the Fourier average amplitude spectrum in Figure 7b. Frankly small-amplitude high-frequency noise in the post-filter shot data (Figure 7c) is attenuated, and therefore the signal-to-noise ratio of the data in general increases, and in particular the reflection are strengthened (Figure 7b).

After filtering the shot records, a predictive deconvolution with a first estimation length of 6 ms and an operator length of 80 ms was applied to dampen the repeated reflections (Figure 8). Since the noise amplitudes especially in the high frequency limits outside the useful band of the data increase after the predictive deconvolution, a band pass filter was applied to the data at cut-off frequencies of [8,10,70,90] Hz after deconvolution (Figures 9a and 9b). Thus, with the application of deconvolution (Figures 9c and 9d), the multiples were weakened and the vertical

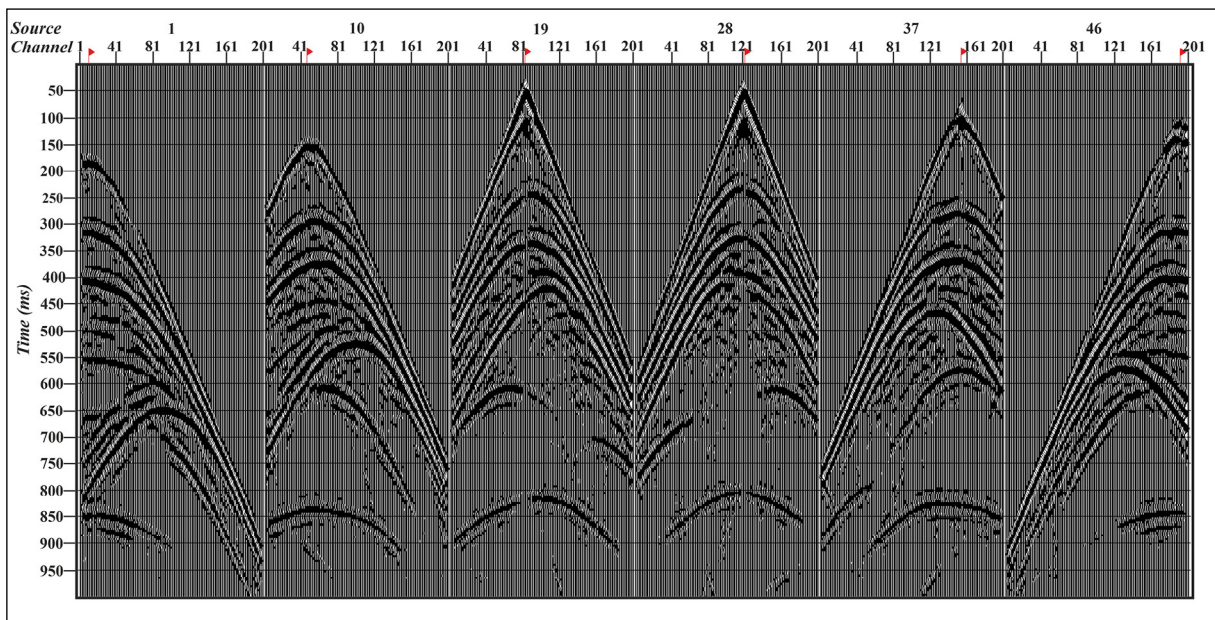


Figure 6- The 1st, 10th, 19th, 28th, 37th and 46th shot groups in which the top cutting process and then band pass filter processes are applied to discard the first arrivals of the granite wash model. The red flag indicates the seismic source (shot point).

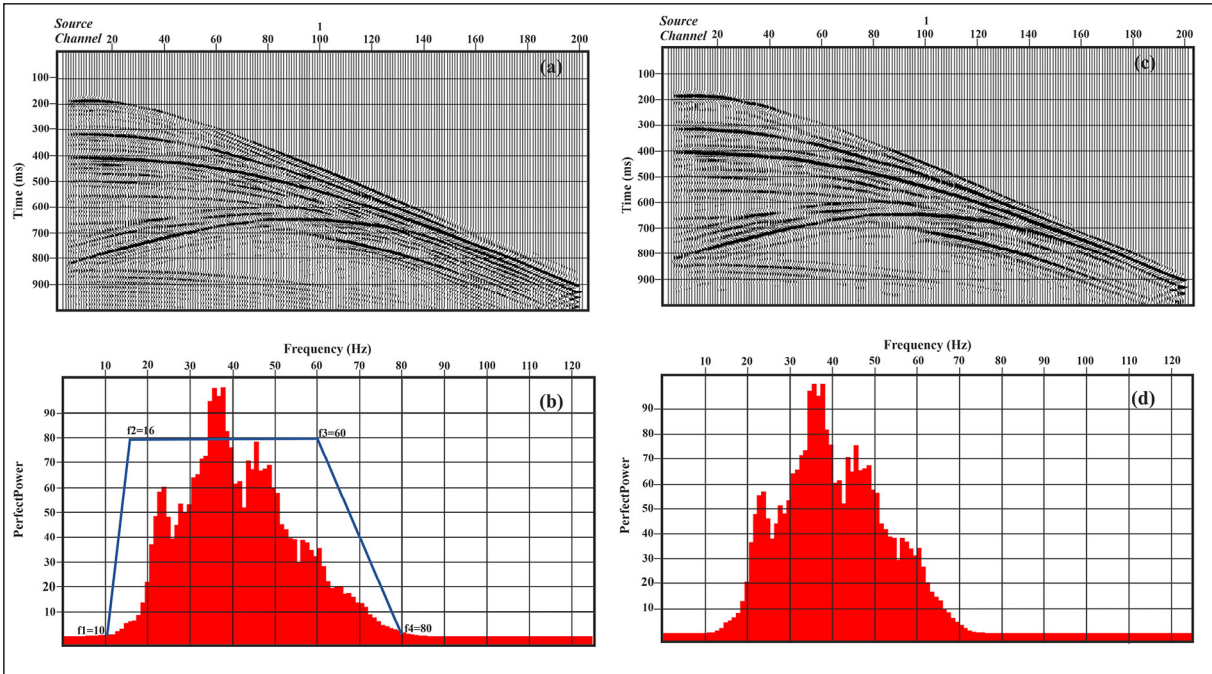


Figure 7- Comparison of the 1st shot recording from granite wash modeling before and after band pass filter. a), b) unfiltered and filtered, and c), d) shot records and Fourier mean amplitude spectra, respectively.

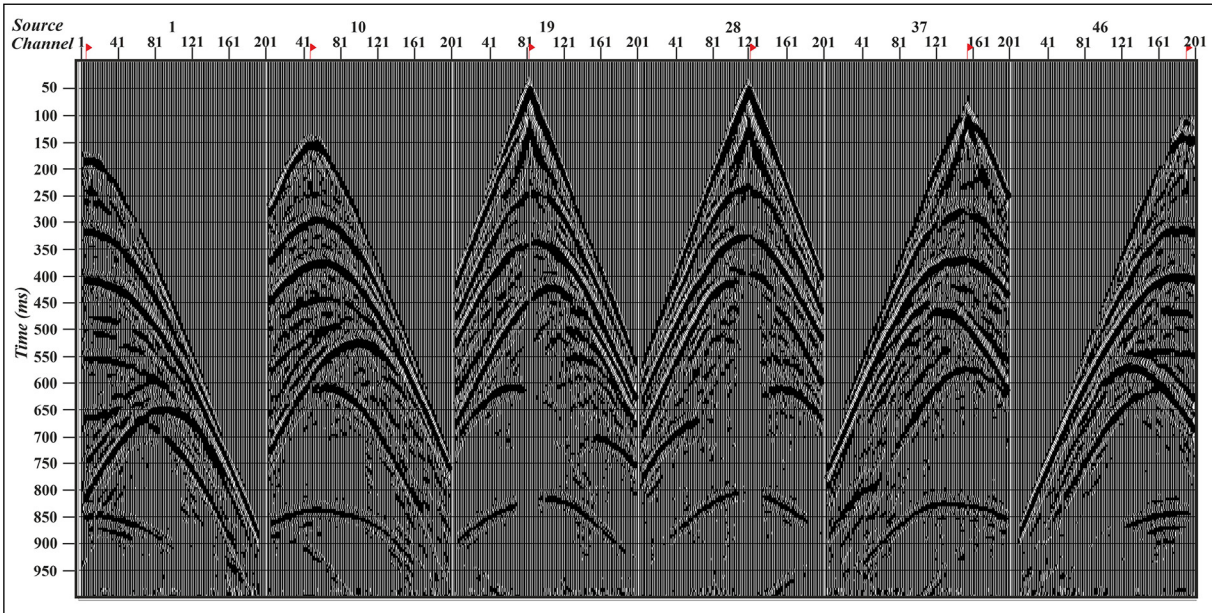


Figure 8- Predictive deconvolution results for the 1st, 10th, 19th, 28th, 37th and 46th artificial shot groups passed through the preliminary data processing stages.

resolution was increased. However, with the help of a band-pass filter, noise is reduced, which is amplified in the high-frequency zone and exerts a distorting effect. In Figure 10, velocity spectrums plots with and without predictive deconvolution applied (left

and applied (right) are given. The velocity spectrum calculation was performed every 20 CMP. Since deep reflections become especially noticeable after deconvolution and their amplitude becomes stronger, the corresponding amplitudes of the speed spectrum

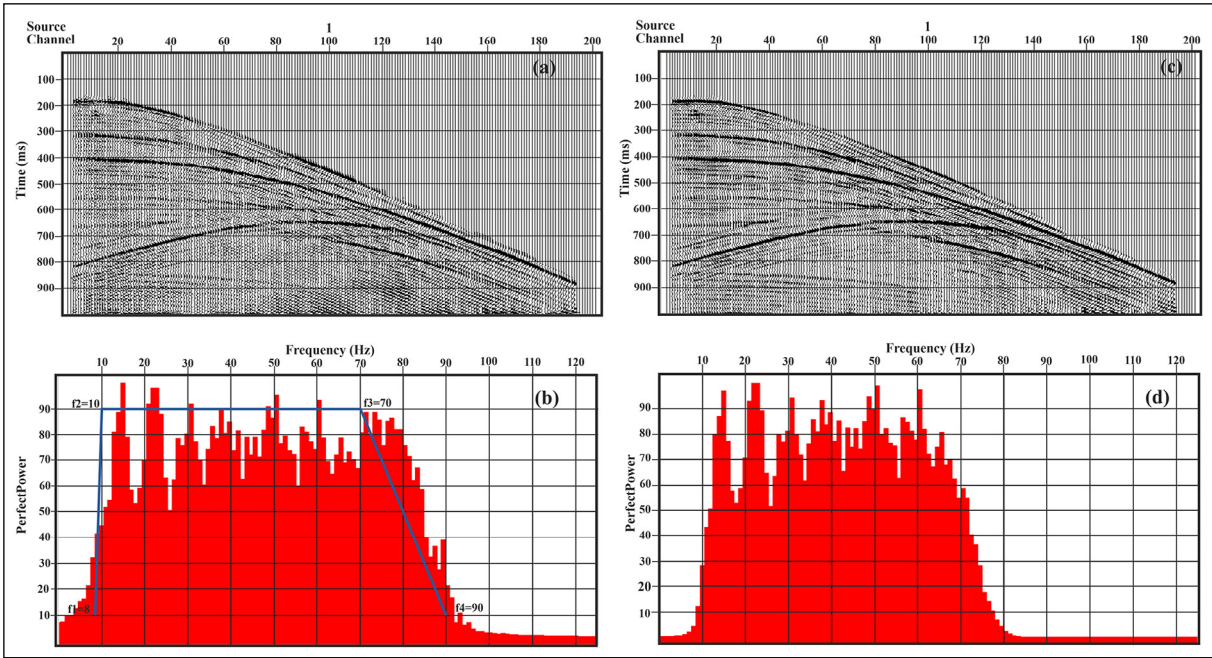


Figure 9- After the predictive deconvolution of the 1st shot recording from the granite wash modeling, the band-pass filter; a) unapplied, b) applied and, c), d) shot records and the amplitude spectra to the Fourier medium.

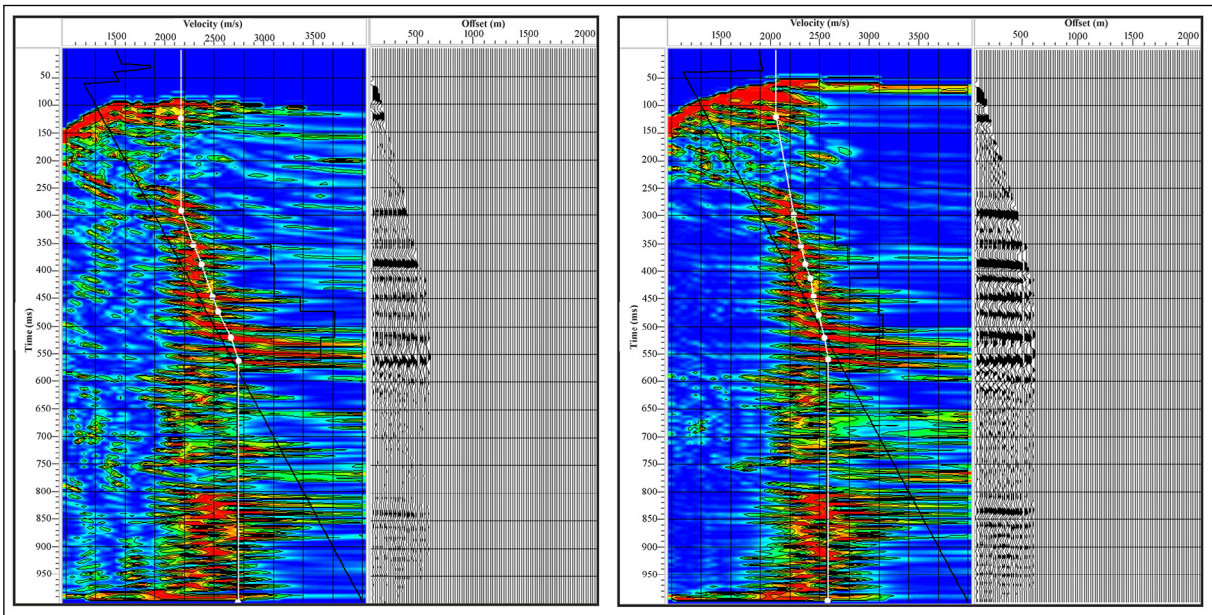


Figure 10- 340. velocity spectrum application on CMP group; a) velocity spectrum images with no predictive deconvolution and, b) applied. The white solid line shows the marked RMS.

are also strengthened at that rate, and therefore the velocity estimation is also made more confidently.

When we look at the CMP section after deconvolution (Figure 10b), it is noteworthy that many reflections in the 300-600 ms range can be seen

differently than those in the CMP cross section in Figure 10a, and especially the presence of reflections in the range of 800-1000 ms. This situation can actually be traced in the velocity spectrum as well. While the velocity picking (white line in Figures 10a and b) was similar on both spectra up to 550 ms, after

that, in the post-deconvolution velocity spectrum, the contours were shifted to higher velocities. Therefore, the predictive deconvolution provided both an increase in the stacking quality and a more accurate determination of the velocity field. Thus, velocity estimates were improved by the deconvolution process, and the determined RMS velocities were applied to the CMP groups, and the NMO corrected CMP groups were obtained. At this stage, the rate function of each CMP is combined to create a speed field for the migration process that will be applied at the next stage. However, in order to remove the stress fields originating from the NMO from the data, a 60% NMO top-cutting process was applied and a masonry section was obtained.

#### 4.2. Processing of Normal Fault Trap Model Data

In normal fault trap modeling, 25 synthetic shot records were obtained and processed according to the workflow specified in Table 2. First, primarily waves were tried to be cleaned by cutting from the top (Figure 11). In the shots on the upper block side of the fault (19 in Figure 5 and 25th. 3) since the reflectors are close to the surface, the reflections are highly interferential with the first arrivals, therefore, direct arrivals could not be completely deleted in these shots, especially in

the sections after 100ms. At the next stage, a band-pass filter with cut-off frequencies of [12, 18, 55, 70] Hz was applied to suppress low-and high-frequency process noise (Figure 11). The results of the time and spectral window of shot data 1 as an example for comparison before and after the filter are shown in Figure 12. According to the Fourier average amplitude spectrum of the input data in Figure 12a (Figure 12b), the useful spectral band of the data is between 18-55 Hz. Accordingly, the filter cut-off frequencies are set to [12 18 55 70] Hz so as not to change this part of the data and are shown in the figure (with a blue line). The time section of the filter result is shown in Figure 12c and the Fourier average amplitude spectrum is shown in Figure 12d. Although both time sections and spectral results do not show a significant difference in comparison, in fact, especially high-frequency small-amplitude vibrations outside the band (see it can be observed that it decays from 500 to 600 ms).

Figure 13 shows the result of applying predictive deconvolution, the operator length of which is 80.0 ms and the prediction distance is 7 ms, to the shot data applied during the preliminary data processing stages. Thus, by attenuating the multiple reflections that are likely to occur, a contribution was made to the velocity

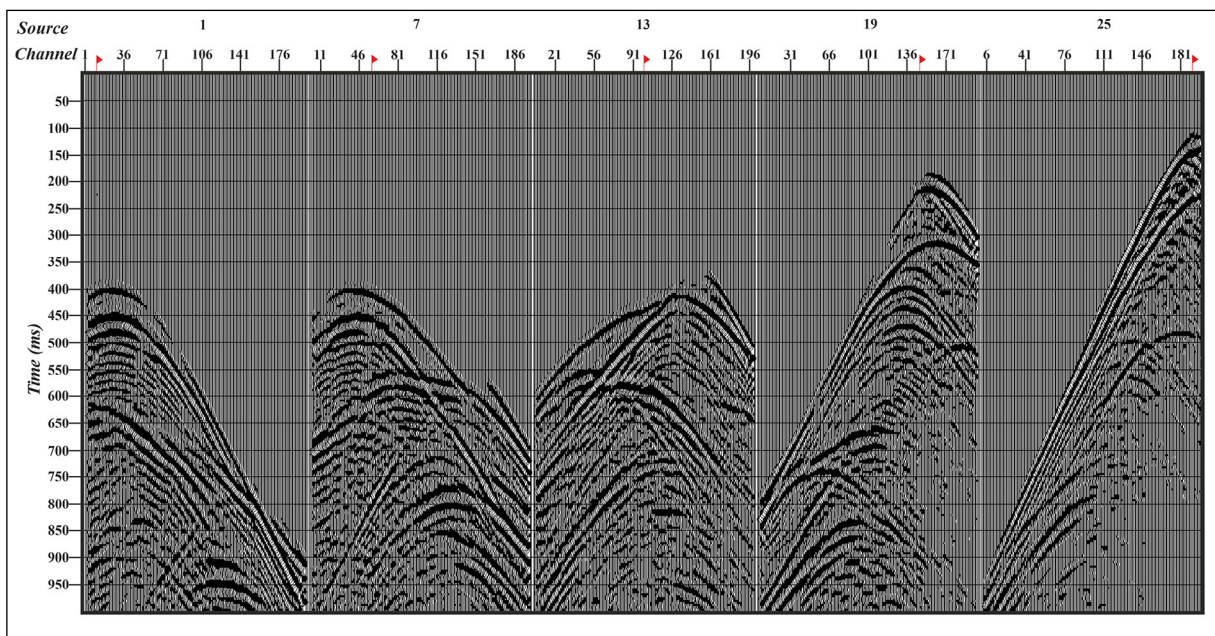


Figure 11- The 1st, 7th, 13th, 19th and 25th shot groups, in which the top shear process is applied to discard the first arrivals from the artificial data of the normal fault trap model, and the band pass filter processes are applied in the following stage. The red flag symbol represents the seismic source (shot point).

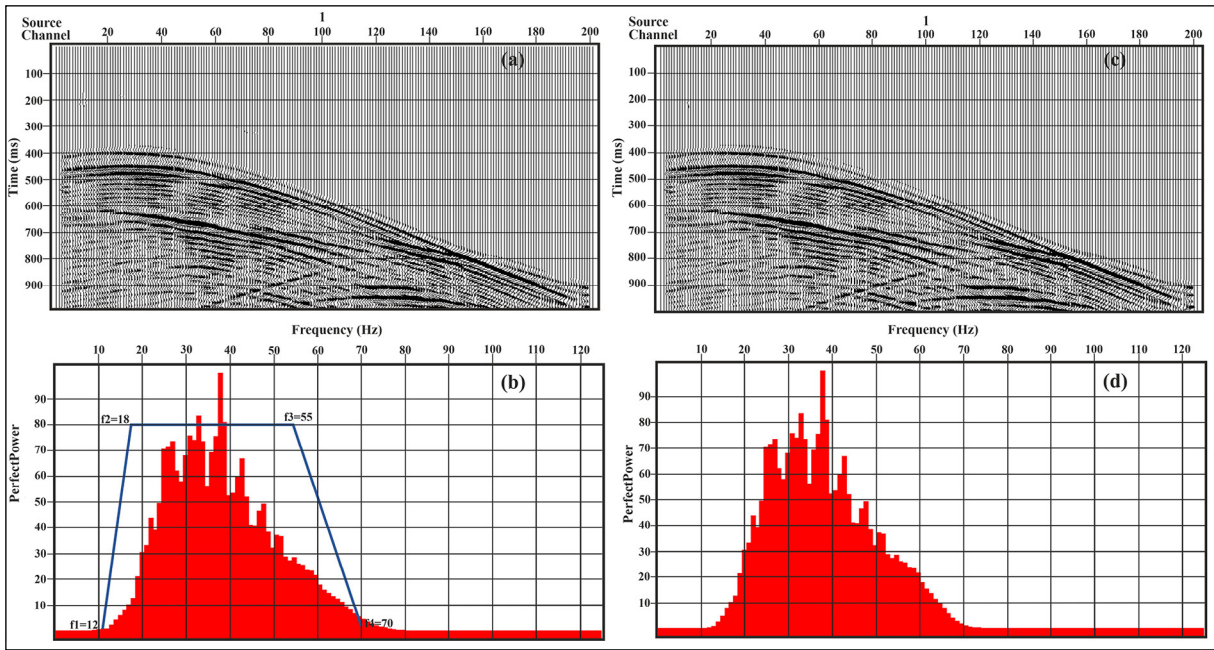


Figure 12- Comparison of the 1st shot recording before and after the bandpass filter; a), b) unfiltered and c), d) filtered shot records and Fourier mean amplitude spectra, respectively.

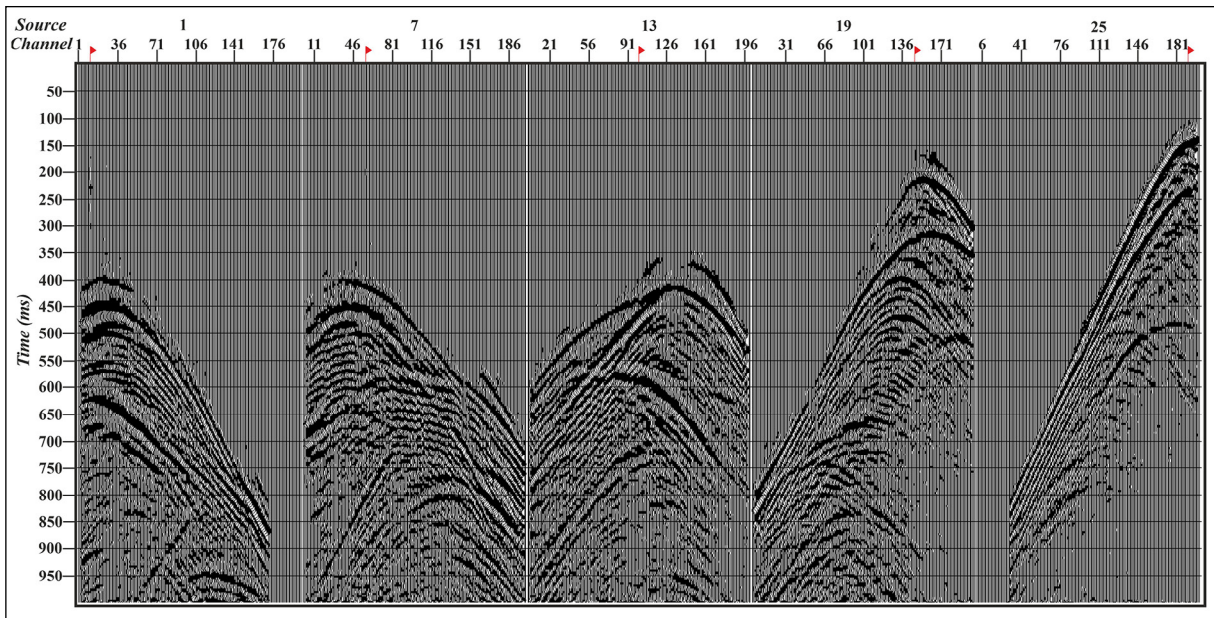


Figure 13- Predictive deconvolution application with operator length of 80.0 ms and prediction distance of 7 ms for the 1st, 7th, 13th, 19th and 25th artificial shot groups passed through the preliminary data processing stages.

estimation and recognition of primary reflections in the velocity spectrum.

In the next processing step, the data was transferred from the shooting environment to the common midpoint environment by the sorting process. At this

stage, it was preferred to use the expression common midpoint (CMP) instead of the common depth point (CDP) for the trace families that will be formed by the traces that are considered to be reflected from the common point. Because the common point traces are made according to the midpoint of the source-receiver

distance on the surface by sorting process. Also, if the reflector is inclined, the common depth point rule does not occur, and reflections occur from the upslope. Thus, velocity analysis was applied to these groups by creating CMP trace groups and 330 at about 1750 m of the normal fault trap model, the CMP trace group is shown in Figure 14. The resulting image is actually an input-output energy ratio-based velocity spectrum (semblance) process, and the most accurate velocity selection (RMS values) over this spectrum is performed visually interactively and the stacking process is performed. The correct choice of speed will ensure the success of the NMO. However, due to the complexity of the data, the stressed areas from NMO were deleted prior to stacking (Figure 14 - right). By combining the obtained velocity functions for each CMP group, the velocity field is obtained, and this velocity field was used in the post-accretion migration stage. A post-accretion Kirchhoff time migration was applied to the obtained accretion data and the

time axis of the cross-section was converted to depth using RMS velocities to compare the main reflection levels in the obtained migration cross section. AGC (automatic gain control) was applied by selecting the window length up to a quarter (1/4) of the data recording time for display purposes.

### 5. Findings

The main purpose of the study was to compare the compatibility of the initial geological model with the migration cross section that will be obtained by calculating the artificial seismic shot records of a complex geological structure containing hydrocarbons and processing these shots with data processing applications, so the findings are given in this context. For the granite wash model ground structure, a Kirchhoff time migration was applied to the stack section produced by the processing steps in Table 2, and then the migration cross section in depth obtained by applying a depth conversion is also given in

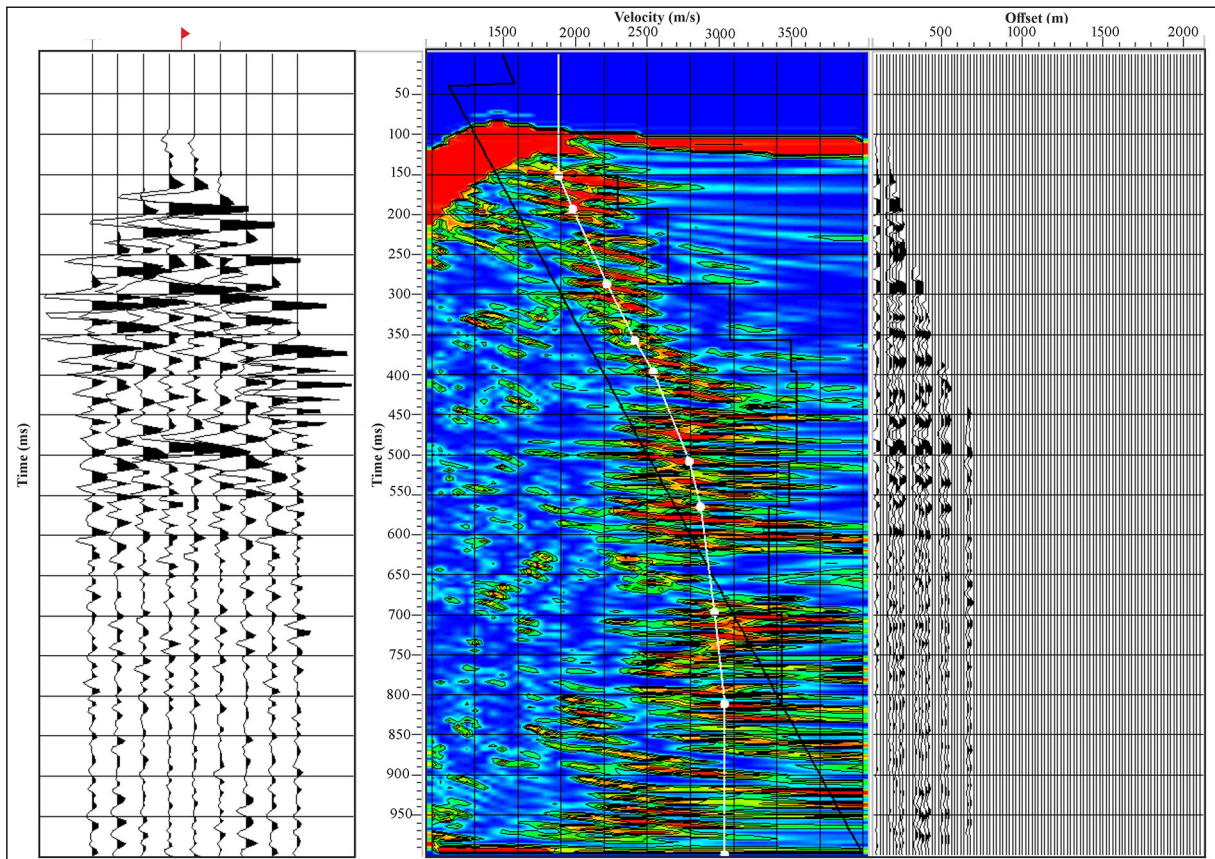


Figure 14- Velocity analysis application on the 330 - CMP group after deconvolution. 330 - CMP traces (left), velocity spectrum image (middle), and view of the CMP group with NMO correction applied (right).

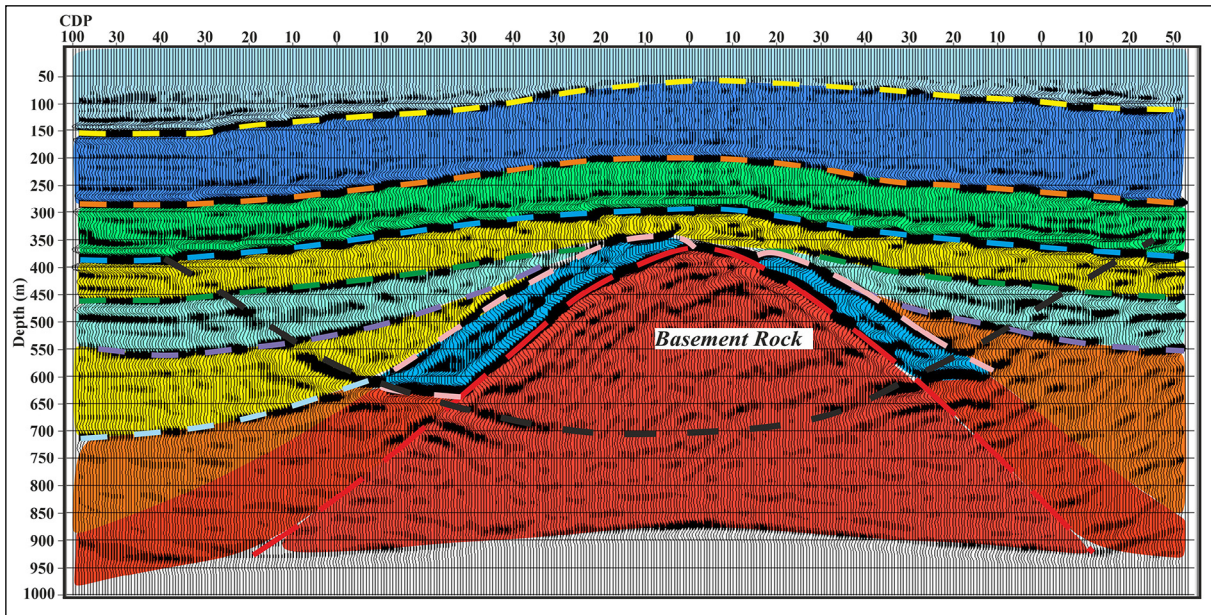


Figure 15- Migration section obtained by applying Kirchhoff time migration and seismic depth conversion after stacking. The main layers are indicated by dashed lines on the section.

Figure 15. The migration step is a process in which scattering and reflections are moved to their real places and almost a real ground model is produced when applied with the correct velocity values and with the appropriate technique. The reflected layers on the migration cross section given in Figure 15 are defined and shown with dashed lines. It can be seen that there is generally a good similarity between the seismic migration section and the ground model in Figure 2. When the migration cross section in Figure 15 was examined, the upper reflectors between 150-400 m depth were continuous, and the granite wash structure between 450 m and 1000 m depth and the trap structures on the right and left sides of the granite wash structure between 450-650 m depth could be determined positional. When evaluated in this context, it was seen that the initial geological model containing the interpreted section and the hydrocarbon trap was in very good harmony. However, the thinning of the thickness of the units towards the top of the granite creates a problem of both vertical and lateral separation in these parts. From a different view point, although there is no negative effect on the interpretation, the event (black dashed line) seen with a convex hyperbolic shape at the bottom of the section has been evaluated as

an excessive migration error (high velocity condition) that is often encountered in relation to the velocities used in the migration process. However, the fact that the boundaries of the geometrically closed structure could be determined almost immediately showed the success of data processing applications and the suitability of the processing parameters used.

Similarly, the migration cross-section obtained by processing the shot data calculated for the normal fault trap model according to the workflow in Table 2 is shown in Figure 16. In general, the migration cross section obtained with the initial ground model has a good relationship each other and the trap structures and layers are able to determined. However, migration effects have been observed along the fault plane in relation to the fact that the normal fault trap model has produced more scattering (in circles with yellow dots). In addition, the continuity of reflections is interrupted due to the fault in general. In particular, the reflections under the traps located in the lower block of the fault have both their amplitude weakened and the reflection continuity from the upper block has been significantly interrupted. Therefore, whether the reflected levels have a lateral continuity or not may require an interpretation related to the interpreter's experience.

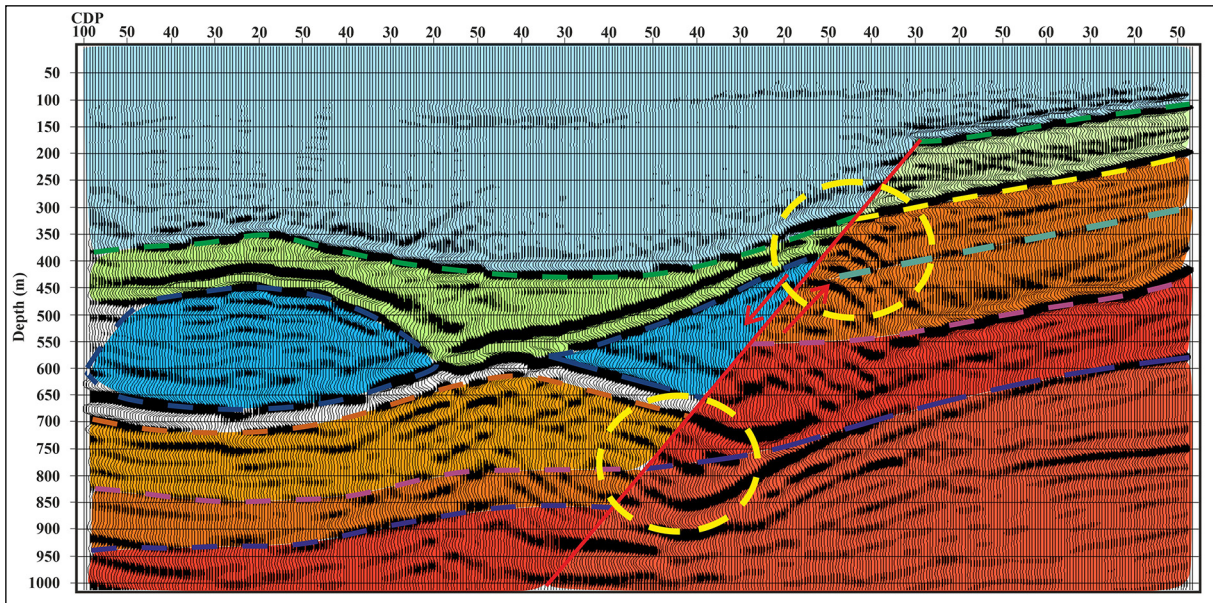


Figure 16- Migration section obtained by applying Kirchhoff time migration and depth conversion after stacking. The main levels are indicated on the section.

## 6. Results

In this article, the seismic reflection reactions of the firing medium of two hydrocarbon traps of the granite wash and normal fault trap types formed in complex geological environments were calculated using the FDM technique, which provides a full-wave field solution. By processing the shot data, the initial ground model and hydrocarbon traps were tried to be displayed. According to modeling studies, i) in the search of thinner and shorter hydrocarbon traps, such as in the granite wash structure, more frequent intermittent shots should be done for reflection record, which will further sample the trap, ii) on the contrary, if the traps associated with faults with a high potential for producing scattering are to be uncovered, a smaller number of shots should be done to reduce the scattering intensity caused to discontinuities. It has been shown that in this way, data collection will be more useful in improving the success of data processing applications and therefore, the image quality of migration sections. However, although artificial data has been used, as is often encountered in the processes of processing real land data, the negative effects of artificial processing noise (in modeling and migration application) (misleading reflection level, reflection migration, reflection distortion, etc.) have been observed on migration cross sections.

However, with the help of data processing applications, the approximate real spatial positions of the layered structure, reflective topographies and trap structures in the initial ground model could be determined on the migration sections obtained in accordance with the obtained migration sections. Therefore, it is proved that the calculation and processing of artificial seismic data on the shot domain for complex underground geological models contributes to the interpretation process. Most especially this modeling approach will be extremely valuable when the interpreter makes estimates of the subsurface geological model and compares the obtained artificial seismic data with seismic data recorded on the terrain. Thus, it is believed that pre-stack shot data modeling, rather than post-stack (zero distance), especially before a decarbon exploration field study, will make a positive contribution to the development of data processing stages and testing of seismic cross-section interpretations.

## Acknowledgements

The authors, one of the judges, contributed to the development of the article with his constructive criticism and suggestions, Prof. Dr. Derman DONDURUR, Prof. Dr. Serkan ÖZTÜRK and another referee who did not reveal his name. In this

study, Matlab code for Finite Difference Modeling of CREWES project is used for free access (<http://www.crewes.ucalgary.ca/>). In order to process the calculated shot records, the Department of Geophysical Engineering of Karadeniz University of technology carried out academic research and use. Promax software of Landmark Graphics Co. donated by Halliburton company is used.

## References

- Ahmadi, O., Juhlin, C., Malehmir, A., Munck, M. 2013. High-resolution 2D seismic imaging and forward modeling of a polymetallic sulfide deposit at Garpenberg, Central Sweden. *Geophysics* 78, 339–350.
- Alaei, B. 2006. Seismic Depth Imaging of Complex Structures, an example from Zagros fold thrust belt, Iran. PhD Thesis, University of Bergen.
- Alaei, B., Petersen, S. A. 2007. Geological modeling and finite difference forward realization of a regional section from the Zagros fold-and-thrust belt. *Petroleum Geoscience* 13, 241–251.
- Alterman, Z., Karal, F. C. 1968. Propagation of elastic waves in layered media by finite-difference methods. *Bulletin of the Seismological Society of America* 58, 367-398.
- Aminzadeh, F., Brac, J., Kunz, T. 1997. SEG/EAGE 3D Modeling Series No 1. Society of Exploration Geophysicists and the European Association of Geoscientists and Engineers.
- Bansal, R., Sen, M. K. 2008. Finite-difference modelling of S-wave splitting in anisotropic media. *Geophysical Prospecting* 56, 293-312.
- Biddle, K. T., Wielchowsky, C. C. 1994. Hydrocarbon Traps, Magoon, L. B., Dow, W. G. (Eds.). *The Petroleum system- from source to traps*. AAPG Memoir 60, 217-234.
- Blake, B., Figueroa, D., Manceda, R., Oller J., Hofland, G. 1999. 3D forward ray trace seismic modeling of strike lines in complex geology. SEG Technical Program Expanded Abstracts, 1871-1874.
- Bohlen, T., Müller, C. F., Milkereit, B. 2003. Elastic wave scattering from massive sulfide orebodies: on the role of composition and shape. In: Eaton, D., Milkereit, B., Salisbury, M. (Ed.), *Hardrock Seismic Exploration*, SEG Developments in Geophysics Series 10.
- Boore, D. M. 1970. Finite-difference solutions to the equations of elastic wave propagation, with application to Love waves over dipping interfaces. PhD Thesis, M.I.T., Claerbout, 1985.
- Carcione, J. M., Herman, G. C., Kroode, A. P. E. 2002. Seismic modeling. *Geophysics* 67, 1304–1325.
- Dec, T., Hein, F. J., Trotter, R. J. 1996. Granite wash alluvial fans, fan-deltas and tidal environments, northwestern Alberta: implications for controls on distribution of Devonian clastic wedges associated with the Peace River Arch. *Bulletin of Canadian Petroleum Geology* 44 (3), 541-565.
- Etgen, J. T., O'Brien, M. J. 2007. Computational methods for large-scale 3D acoustic finite-difference modeling: a tutorial. *Geophysics* 72, 223–230.
- Geiger, H. D., Daley, P. F. 2003. Finite difference modelling of the full acoustic wave equation in Matlab. CREWES Research Report 15.
- Gjøystdal, H., Iversen, E., Lecomte, I., Kaschwich, T., Drottning, A., Mispel, J. 2007. Improved applicability of ray tracing in seismic acquisition, imaging, and interpretation. *Geophysics* 75, 261–271.
- Holberg, O. 1987. Computational aspects of the choice of operator and sampling interval for numerical differentiation in large-scale simulation of wave phenomena. *Geophysical Prospecting* 35, 629-655.
- Huang, Y., Lin, D., Bai, B., Roby, S., Ricardez, C. 2010. Challenges in presalt depth imaging of the deepwater Santos Basin, Brazil. *The Leading Edge* 29, 820–825.
- Hyne, N. J. 1984. *Oil and Gas Field Classifier*, Second edition. PennWell Maps Publishing Company.
- Igel, H., Mora, P., Rioulet, B. 1995. Anisotropic wave propagation through finite-difference grids. *Geophysics* 60, 1203–1216.
- Jinhua, Y., Tao, L., Tianyue, H. 2009. Modeling seismic wave propagation within complex structures, *Applied Geophysics* 6, 30-41.
- Kelly, K. R., Ward, R. W., Treitel, S., Alford, R. M. 1976. Synthetic seismograms: a finite-difference approach. *Geophysics* 41, 2–27.
- Krebes, E. S., Lee, L. H. T. 1994. Inhomogeneous plane waves and cylindrical waves in anisotropic anelastic media. *Journal of Geophysical Research* 99(23), 899-919.
- Lines, L. R., Slawinski, R., Bording, R. P. 1999. Short note: a recipe for stability of finite-difference wave-equation computations. *Geophysics* 64, 967-969.

- Lingrey, S. 1991. Seismic modeling of an imbricate thrust structure from the foothills of the Canadian Rocky Mountains. Fagin, S. W. (Ed.). *Seismic Modeling of Geologic Structures Applications to exploration Problems*. Society of Exploration Geophysicists 111-125.
- Liu, Y., Sen, M. K. 2009. Advanced finite-difference methods for seismic modeling. *Geohorizons*, 5-16.
- Manning, P. M., Margrave, G. F. 1998. Elastic wave finite difference modelling as a practical exploration tool. *CREWES Research Report*. 10, 16.
- Marfurt, J. K. 1984. Accuracy of Finite-Difference and Finite Element Modeling of the Scalar and Elastic Wave Equations, *Society of Exploration Geophysicists*.
- Margrave, G. 2003. Numerical methods of exploration seismology with algorithms in Matlab. <http://www.crewes.org/ResearchLinks/FreeSoftware/>.
- Moczo, P., Robertsson, O. J. A., Eisner, L. 2007. The finite-difference time-domain method for modeling of seismic wave propagation. *Advances in Geophysics* 48, 421-516.
- Morse, P. F., Purnell, G. W. Medwedeff, D. A. 1991. Seismic modeling of fault-related folds. Fagin, S. W. (Ed.). *Seismic Modeling of Geologic Structures: Applications to Exploration Problems*. Society of Exploration Geophysicists, 127–152.
- Nejati, M., Hashemi, H. 2012. Migrated Exploding Reflectors in Evaluation of Finite Difference Solution for Inhomogeneous Seismic Models. *Engineering* 4, 950-957.
- Ottaviani, M. 1971. Elastic wave propagation in two evenly welded quarter-spaces. *Bulletin of the Seismological Society of America* 61, 1119-1152.
- Özbek, A., Vassallo, M., Özdemir, K., Van Manen, D. J., Eggenberger, K. 2010. Crossline wavefield reconstruction from multicomponent streamer data: part 2 - joint interpolation and 3D up/down separation by generalized matching pursuit. *Geophysics* 75, WB69–WB85.
- Robertson, J. O. A., Van Manen, D. J., Schmelzbach, C., Renterghem, C. V., Amudsen, L. 2015. Finite-difference modeling of wavefield constitutes. *Geophysical Journal International* 203, 1334-1342.
- Sayers, C., Chopra, S. 2009. Introduction to special section: Seismic modeling. *The Leading Edge* 28, 528-529.
- Sproule, J. C. 1956. Granite wash of Northern Alberta. *Journal of the Alberta Society of Petroleum Geologists* 4(9), 197-203.
- Talukdar, K., Behere, L. 2018. Sub-basalt imaging of hydrocarbon-bearing Mesozoic sediments using ray-trace inversion of first-arrival seismic data and elastic finite-difference full-wave modeling along Sino r– Valod profile of Deccan Syncline, India. *Pure and Applied Geophysics* 175, 2931–2954.
- TPAO (Türkiye Petrolleri Anonim Ortaklığı). <http://www.tpao.gov.tr/?mod=sektore-dair&contID=97>. 25 April 2022.
- Virieux, J. 1986. P-SV wave propagation in heterogeneous media: Velocity stress finite difference method. *Geophysics* 51, 889–901.
- Youzwishen, C. F., Margrave, G. F. 1999. Finite difference modelling of acoustic waves in Matlab. *CREWES Research, Report No: 11*.
- Zhang, H., Zhang, Y. 2007. Implicit splitting finite difference scheme for multi-dimensional wave simulation. *75th Annual International Meeting, SEG, Expanded Abstracts, 2011-2014*.

